Hindawi
Journal of Chemistry
Volume 2023, Article ID 9890207, 1 page
https://doi.org/10.1155/2023/9890207

Retraction

Retracted: Influence of Electrochemical Anticorrosion Technology on Concrete Structure and Performance

Journal of Chemistry

Received 15 August 2023; Accepted 15 August 2023; Published 16 August 2023

This article has been retracted by Hindawi following an investigation undertaken by the publisher [1]. This investigation has uncovered evidence of one or more of the following indicators of systematic manipulation of the publication process:

(1) Discrepancies in scope
(2) Discrepancies in the description of the research reported
(3) Discrepancies between the availability of data and the research described
(4) Inappropriate citations
(5) Incoherent, meaningless and/or irrelevant content included in the article
(6) Peer-review manipulation

The presence of these indicators undermines our confidence in the integrity of the article's content and we cannot, therefore, vouch for its reliability. Please note that this notice is intended solely to alert readers that the content of this article is unreliable. We have not investigated whether authors were aware of or involved in the systematic manipulation of the publication process.

Wiley and Hindawi regrets that the usual quality checks did not identify these issues before publication and have since put additional measures in place to safeguard research integrity.

We wish to credit our own Research Integrity and Research Publishing teams and anonymous and named external researchers and research integrity experts for contributing to this investigation.

The corresponding author, as the representative of all authors, has been given the opportunity to register their agreement or disagreement to this retraction. We have kept a record of any response received.

References

[1] Q. Yang, "Influence of Electrochemical Anticorrosion Technology on Concrete Structure and Performance," *Journal of Chemistry*, vol. 2022, Article ID 5702379, 7 pages, 2022.

Hindawi
Journal of Chemistry
Volume 2022, Article ID 5702379, 7 pages
https://doi.org/10.1155/2022/5702379

Research Article

Influence of Electrochemical Anticorrosion Technology on Concrete Structure and Performance

Qin Yang

Henan College of Transportation, Zhengzhou, Henan 450000, China

Correspondence should be addressed to Qin Yang; 0107025@yzpc.edu.cn

Received 15 July 2022; Revised 14 August 2022; Accepted 17 August 2022; Published 30 August 2022

Academic Editor: Ajay Rakkesh R

In order to solve the problem of steel bar desensitization in island concrete, which leads to steel bar corrosion and greatly reduces the service life of structures, this work studies the influence of electrochemical corrosion prevention technology on the structure and performance of concrete. Through linear sweep voltammetry (LSV) and electrochemical impedance spectroscopy (EIS), the reinforcement in seawater sand concrete and ordinary concrete under two different chloride ion erosion modes was tested electrochemically, and then, its polarization curve and electrochemical impedance spectrum were obtained and analyzed. The experimental results show that the slope ratio of anode Tafel decreases significantly under the condition of steel bar passivation. The self-corrosion potential of reinforcement is −204 MV, which is much higher than −480 MV obtained from early testing. The self-corrosion potential obtained from the L3 polarization test tends to be stable after 84 days. As the test continues, the capacitive reactance arc in L1 and L2 medium-frequency region will gradually disappear with the continuous development of corrosion. *Conclusion*. This study explains the electrochemical mechanism and rate of reinforcement corrosion in seawater and sea sand concrete.

1. Introduction

Concrete is made from cementitious materials, aggregates, water, and admixtures in one proportion. Depending on the needs of the project, some necessary additions and additives can be added to improve the performance of the stone. Stone materials have a variety of raw materials, low cost, stone has good plasticity, is resistant to compression, and can be used in combination with steel. Therefore, stone is one of the most widely used materials in civil engineering [1]. With the continuous improvement of construction in China, the construction of major projects such as Hong Kong Zhuhai Macao Sea Crossing Bridge, Shanghai Port, and Qinghai Tibet Railway will not only lead to development of the country "Belt and Belt" but also the roadmap concept, along with China's global strength. However, the environment around these large-scale projects is difficult, and the operation seems to be poor due to the impact. For long-term environment and transportation, engineering investigation shows that the service life of marine concrete structures is about 50–100 years. However, many concrete structures enter the aging period after 20 years of service, resulting in steel corrosion and other damage [2, 3]. These losses result in high financial losses, and these losses are greater than the actual cost of the project. In 2015, the Chinese Academy of Engineering implemented a large-scale technical project "China's corrosion prevention" and conducted specialized research in China's infrastructure, transportation, and other sectors. According to research, in 2014, the total cost of corrosion in China was 2.13 trillion yuan, accounting for 3.34% of the annual total products in the country.

2. Literature Review

Yu et al. used EIS to study the influence on the corrosion behavior of reinforcement in reinforced concrete structures. It is found that the impedance of steel bar shows the capacitive reactance characteristics under high frequency and low frequency, corresponding to two time constants, corresponding to electric double layer and passive film,

respectively. At the same time, the arc of the low-frequency response capacitance is flat, which shows that the charging and discharging of the two-phase voltage is not charging and discharging the equipment. Electricity is ideal, and there is a difference between the two. This is mainly due to the unevenness of the steel surface. After soaking for some time, the tail diffusion appears in the region less often, and the exchange rate refuses to decrease by two orders of magnitude, which is due to the damage in villages of passive film, which makes it low. Prevent the effect of reinforcement; corrosion of reinforcement is greatly affected by enrichment. As the concentration increases, it is easier to damage the passive film and the corrosion improvement is faster; At the same time, the author also discussed the changes of electrochemical parameters such as corrosion potential, charge transfer resistance, and Warburg impedance in the process of reinforcement corrosion [4]. Dong et al. studied the EIS characteristics of the corrosion process of reinforcement in simulated concrete pore fluid. The experimental results show that with the addition of simulated concrete pore fluid, the change characteristics of reinforcement impedance obviously show three completely different stages. In the corrosion system studied, there is a critical value of concentration. When the concentration is lower than the critical value, the passive film will not be destroyed, and the surface of the steel bar is completely passivated. The electrochemical impedance spectrum shows the characteristics of a capacitive reactance arc with a large radius. When the concentration is higher than the critical value, the radius of capacitive reactance arc decreases significantly, while the inductive reactance arc appears in the low-frequency region, and the charge transfer resistance also decreases sharply. In the last stage, the electrochemical impedance spectroscopy shows the characteristics of two time constants. Steel bars show different electrochemical impedance characteristics in the passivation stability period, pitting induction period, and pitting development period, and the time constant also changes continuously. At the same time, the charge transfer resistance decreases with the increase of concentration and with the decrease of pH value, which indicates that the corrosion rate of reinforcement is affected by both pH value and concentration [5]. Yu et al. used EIS to study the corrosion behavior of reinforced concrete structures in solution. The experimental results show that at the beginning of immersion, a capacitive reactance arc with a large radius appears on the Nyquist diagram of the electrochemical impedance spectrum, which indicates that at this time, the passive film has a good protective effect on the reinforcement, and the surface passivation of the reinforcement is good. After soaking for a period of time, the Nyquist diagram of the electrochemical impedance of the reinforcement shows the characteristics of two capacitive reactance arcs, which indicate that the passivation meter on the surface of the reinforcement has begun to damage, and the reinforcement matrix has begun to corrode. The appearance of the low-frequency capacitive reactance arc indicates that the charge transfer process has begun to occur on the surface of the reinforcement, that is, the reinforcement has begun to corrode and dissolve. When the immersion reaches the later stage, the Nyquist diagram shows the diffusion tail, showing the characteristics of Warburg impedance, which shows that at this time, the corrosion is no longer controlled by the charge transfer process, but by the diffusion process. In the whole process, the capacitive reactance arc radius of EIS decreases gradually, which indicates that the corrosion of reinforcement is becoming more and more serious. At the same time, the author also studied the influence of pH value and concentration on reinforcement corrosion [6]. Dong et al. used EIS to study the corrosion behavior of concrete in simulated rock pore fluid with different pH in dry-wet alternating conditions. According to the test, the corrosion process of steel bars can be divided into three stages, namely, passive film dissolution stage, corrosion activation stage, and corrosion product accumulation stage. When the pH value of the solution is 1, the reinforcement mainly shows uniform corrosion behavior, while when the pH value of the solution is 3 or 7, the reinforcement mainly shows small hole corrosion behavior. The results of EIS further confirmed the existence of three stages. In the first phase, the electrochemical resistance spectrum consists of high-frequency capacitive field arcs and low-frequency capacitive field arcs and exhibits the characteristics of two-phase continuous. At this time, the capacitive reaction arc of the final frequency is an indication of the electrochemical resistance of the passive film, and the capacitive reaction arc of the minimum frequency is the embodiment of the double voltage, set of transfer fees. In the second step, electrochemical impedance spectroscopy was observed three times, that was related to the continuity of the corrosion material in steel bars. In the third stage, the arc radius of the capacitance reaction in the medium frequency is much reduced, which indicates that the corrosion protection material continues to penetrate into the rock. Then, as cl concentration increases and pH value decreases and the corrosion improvement becomes more and more severe [7].

This paper examines the effect of chlorides carried on by the aggregation and mixing of water on the substrate and after the passivation of the adsorbent. Combined with the protection spectrum obtained by the experiment, an equivalent model of corrosion improvement occurs from chloride ions at different times, and then, the process of improvement corrosion in seawater and sand-reinforced rocks is caused by electrochemical exposure. Figure 1 shows the content and process of this form.

3. Research Methods

3.1. Material and Fabrication of Test Piece. The strength level of the concrete test is C30. The coarse aggregate for sea sand-reinforced rock samples is undesalinated sea rocks with a grain size of 5–20 mm. The fine aggregate was sieved sea sand with a fineness modulus of 2.8 and a chloride ion content of 0.24%. The mixed water is formed by the oceans. Coarse aggregates for ordinary strength design are ordinary crushed stone, the size of which is 5–20 mm. The fine aggregate is natural sand sieved with a fine modulus of 2.65, and the water mixture is tap water [8, 9]. The equations of the two mixtures are the same, see Table 1 for details. The tests are

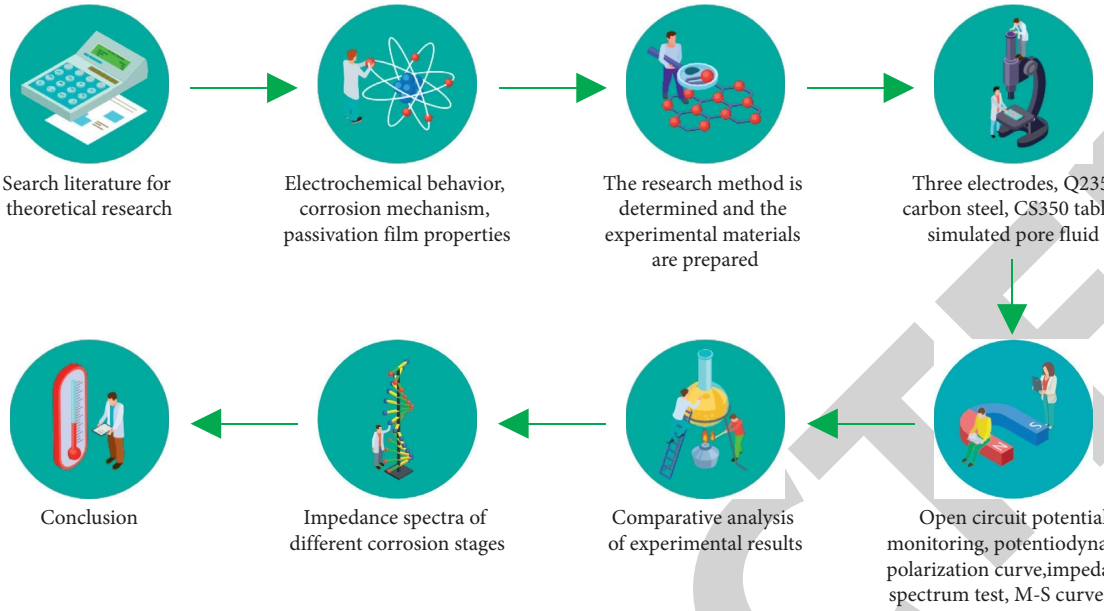

Figure 1: Article content process.

Table 1: The concrete mix proportion.

Cement/ (kg/m^3)	Water/ (kg/m^3)	Sand/ (kg/m^3)	Stone/ (kg/m^3)	Water cement ratio
496.03	203.37	520.83	1279.76	0.41

concrete and marine rocks with dimensions × width × height = 100 mm × 100 mm × 100 mm. During casting, the rebar is embedded in the concrete electrode and 304 stainless steel is used as the auxiliary electrode. The thickness of the reinforcement protection layer is 2 cm, and the diameter between the reinforcement and stainless steel is 12 mm. A PVC pipe with a diameter of 10 cm is placed on the concrete structure and sealed with epoxy resin [10]. Inject the prepared artificial seawater into the PVC container for chloride ion penetration, connect the exposed part of the reinforcement and stainless steel with wires, and seal the remaining five surfaces of the concrete specimen with epoxy resin.

3.2. Grouping and Curing of Test Pieces. After the samples were designed and dried for 28 days, artificial seawater was put in, and a team used new film to close the hole to simulate an underwater environment. The other is to pour the ocean water after 2 days, dry it outside in the air for 3 days, and then put it in artificial water to simulate a tidal environment. The environmental performance measurement is (20 ± 5)°C. L1 and L2 are ocean rocks and L3 and L4 are white rocks and soak and dry with a wet-dry circle.

3.3. Electrochemical Test

3.3.1. Polarization Curve Test. A three-electrode system is used in electrochemical experiments. The instrument electrode is an electrochemical workstation AUTOLAB-AUT86742 developed by Wantong Co., Ltd., Switzerland, and the material used for the electrode is saturated calomel electrode [11].

3.3.2. EIS Test. The measurement of electrochemical impedance spectroscopy was completed by the AUTOLAB-AUT86742 electrochemical workstation produced by Swiss Wantong Co., Ltd. The AC excitation signal adopts sine wave signal, the frequency range is 106~10–3 Hz, the amplitude is 10 MV, the reinforcement potential is controlled as open circuit potential during the test, and the test environment of the test piece is controlled at (20 ± 5) [12]. ZsimpWin software is used to process the impedance data of the specimen, analyze the structure of the equivalent circuit model and the parameters of each component, and use different equivalent circuits to fit according to the different corrosion conditions of the system.

4. Result Analysis

4.1. Polarization Curve Behavior. Figure 2 shows the polarization curve of corroded reinforcement in the test piece [13]. At this time, the polarization curve characteristics of the four specimens at this time are basically the same, and the curve has two obvious characteristics: first, the slope of the anode polarization curve is gentle, and the slope of the curve is small, that is, the slope β_a of the anode Tafel is significantly reduced when the reinforcement is passivated, and the anode dissolution reaction of the electrode can proceed smoothly, indicating that the reinforcement is currently in a corroded state. Second, it can be seen from the polarization curve that the self-corrosion potential $\mathbf{E_{corr}}$ of

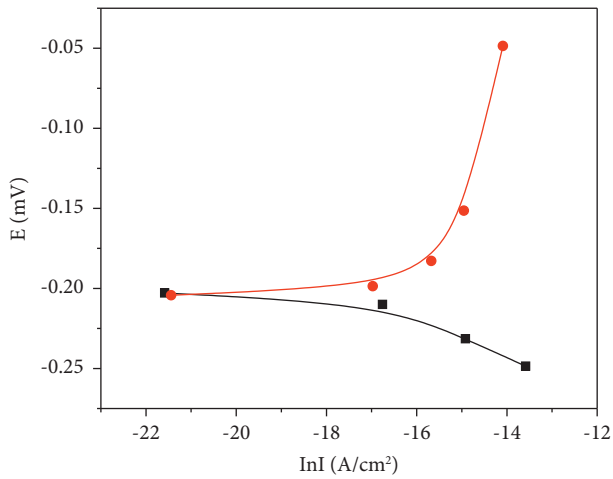

Figure 2: The rebar polarization curve of specimen L2 at 336 D.

the reinforcement at this time is −204 mV, which is much higher than the −480 mV obtained in the early test.

Figure 3 shows the change in self-corrosion capacity of the test section. In the first part of the experiment, it was found that the self-corrosion resistance of L3 and L4 reinforcements was lower than that of L1 and L2, which showed that the difference between the anode and cathode was larger and that the support is prone to corrosion. Seawater and sand concrete are obvious references of chlorides in aggregate and mixed water [14]. Reflected in the polarization curve, the self-corrosion capacity gradually increases, that is, the hardness of steel corrosion gradually increases in the next phase [15]. It is worth noting that the self-corrosion potential of L3 tends to be flat from 84 D. Combined with its impedance spectrum, we infer that since L3 is a specimen immersed in artificial seawater, it is difficult for oxygen to diffuse into it, and there is no chloride ion in the concrete mixing water and aggregate. In addition to the existence of the concrete protective layer, the chloride ion diffusion in the concrete is slow, and the thickness of the corrosion products generated by the reaction is also the thinnest among all the test pieces. For the time being, the protection effect on the reinforcement surface has not been formed, and the electrochemical corrosion on the reinforcement surface is still in the mode of large cathode and small anode. Therefore, the self-corrosion potential obtained from L3 polarization test tends to be stable after 84 days.

4.2. Electrochemical Impedance Behavior. In the study of electrochemical impedance spectroscopy, there are mainly two kinds of analysis diagrams, one is called Nyquist diagram, which is called Nyquist diagram for short, and the other is called Bode figure [16]. The vertical axis of the Nyquist diagram is the imaginary part Z_{Im} of the linear circuit impedance in the polarization system, and the horizontal axis is the real part Z_{Re} of the impedance. From the basic principle of EIS, we can get the real part Z_{Re} and the imaginary part Z_{Im} satisfy the relationship of the following formula:

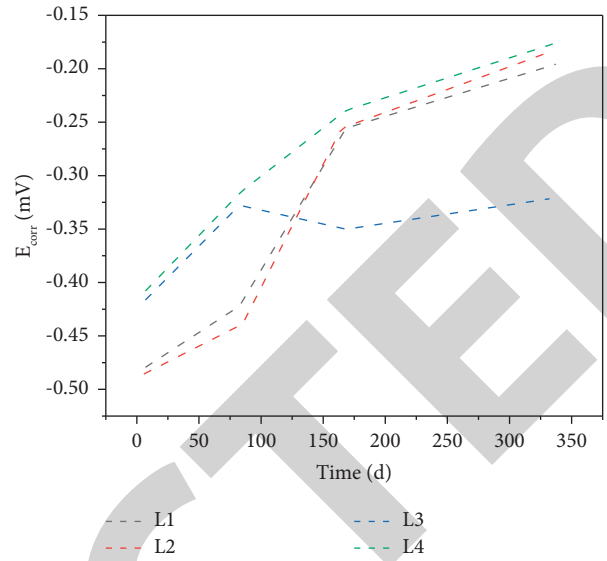

Figure 3: Change of self-corrosion potential of reinforcement with time.

$$\left(Z_{\mathrm{Re}} - \frac{R_t}{2}\right)^2 + Z_{\mathrm{Im}}^2 = \left(\frac{R_t}{2}\right)^2, \tag{1}$$

where R_t describes the resistance of the equivalent element of the Faraday process on the electrode surface.

It can be seen that in the Nyquist diagram, this is a circle with $(R_t/2, 0)$ as the center and $R_t/2$ as the radius. It can be seen that the radius of the semicircle characterized in the impedance spectrum can be used to preliminarily compare the impedance of the equivalent capacitance element.

Figures 4(a) and 4(b) show the EIS diagram of the electrochemical impedance response of carbon steel electrode in seawater and sand concrete at different stages. Through comparison, we found that at this time, because the chloride ion in the artificial seawater has a shallow erosion depth, it has not contacted the reinforcement in the test piece at all, and the different erosion environment has not affected the development of the passive film on the surface of carbon steel for the time being. There are only chloride ions contained in the aggregate surface and mixing seawater around the reinforcement, so the Nyquist diagrams of L1 and L2 in the first week are completely consistent [17, 18]. In further experiments, the arc resistance of L1 and L2 capacitances in the frequency range was the difference of 84 days, indicating that during this time, the effects of differential corrosion of carbon steel begins to appear slowly. The fluidity of the whole process of corrosion protection and the migration capacity of the corrosion protection material is very weak, so the control level of the whole process is diffusion capacity of corrosion protective equipment [19].

Figure 5 shows the 84th day impedance spectrum of each specimen. By analyzing the images of L3 and L4, they found that capacitive reactance arcs also appeared in the mid-frequency range. Capacitive reactance arcing in the medium frequency is associated with pitting corrosion of steel surfaces [20]. Compared with Figure 1, as the test continues, the capacitive reactance arc at intermediate frequency L1 and L2

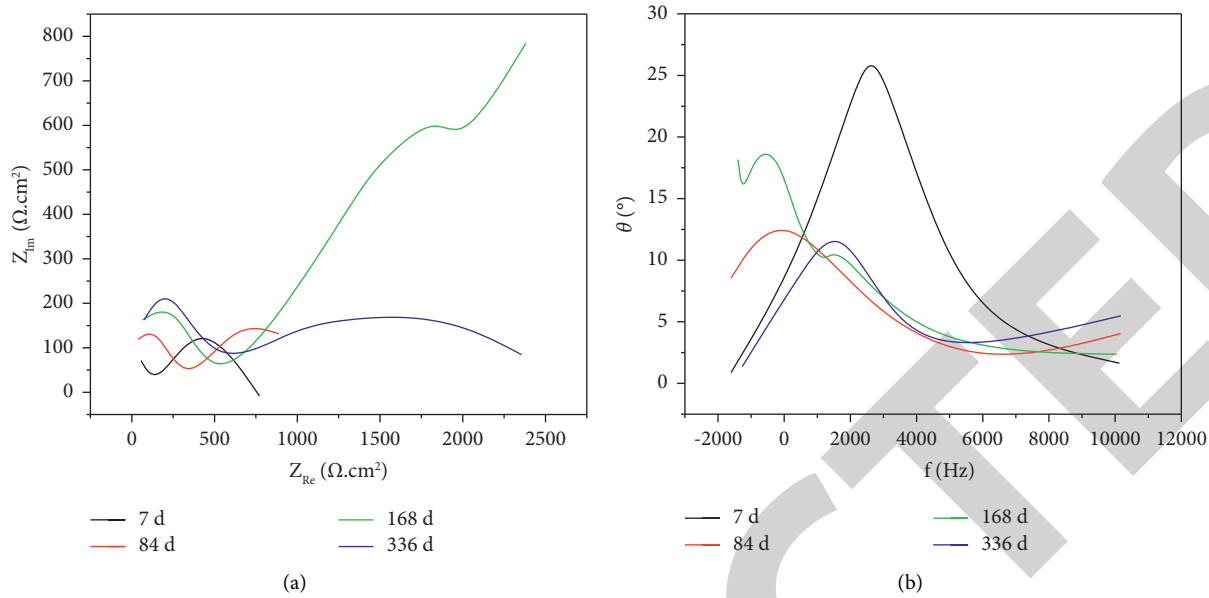

Figure 4: Nyquist diagram and Bode diagram of specimen L2.

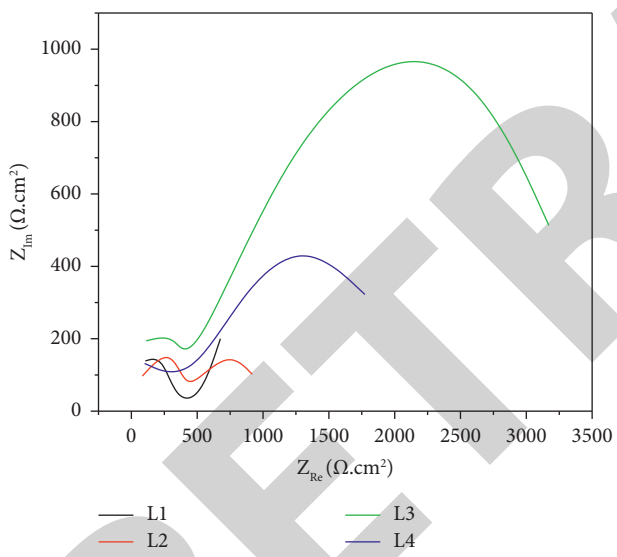

Figure 5: Nyquist diagram of the test piece at 84 D.

gradually disappears with continuous corrosion. We conclude that the occurrence of capacitive reactance arc in this section is due to the Faraday process of dissolution of iron at the bottom of the corrosion hole on the surface of the steel bar. In the first stage, there is high chloride content in the test strips and water mixture, which has a positive effect on the passive film of carbon steel. At 84 days, the effect of pitting on the surface of the steel bar begins to develop everywhere, the effect of cathode large and small anode is weak, the anode current speed of corrosion prevents the gradual decrease, and the effect of ohmic decline gradually weakens. The capacitive field arc in the medium-frequency region of the seawater and sand group is shown in the figure before disappearing, and the resistance in the low-frequency region is simultaneously lower than that of the white rock pile.

It is worth noting that we can clearly see from Figure 5 that while the capacitive reactance arc radius in the low-frequency region of L1 is smaller than L2, L3 is larger than L4. The electrochemical characterization of the above two points is that the capacitive reactance arc radius is larger [21].

4.3. Equivalent Circuit Model. From the chlorine salt corrosion Nyquist diagram above, when the armature is in the passive state (day 7), the Nyquist diagram has two capacitive reactance arcs, i.e., two constant times. When the armature is in the activated state (day 84), the capacitive reactance arc in the medium-frequency range, i.e., three times constant, is added [22]. Based on this, we conclude that the equation model in the two states is shown in Figures 6(a)-6(b), respectively.

Following the model of the experimental model and previous experience, we believe that in a similar picture of this experiment, R1 represents the solution, R2 represents the protection of the protective layer, and R3 represents the exchange rate of the protective material. The process is complete. Reinforcement at the bottom of the borehole: R4 represents the conduction resistance of two electrical layers on the surface of the reinforcement, and W represents the diffusion-related element (Warburg resistance) in the same the circuit, simulating the diffusion control effect. At this time, the passive film at the center of the support is broken, and it changes from a stable passive to a corrosively state. At this point, controlling the steps in the entire corrosion protection process is not a substitution process, but rather a major change process of the corrosion protection process or product [23, 24]. The experimental receiving impedance spectra shows that the image of most capacitive reactance arcs is flat rather than the ideal semicircle, which is called the dispersion effect. In the case of hard rocks, this phenomenon is related to the variability of the metal surface and the

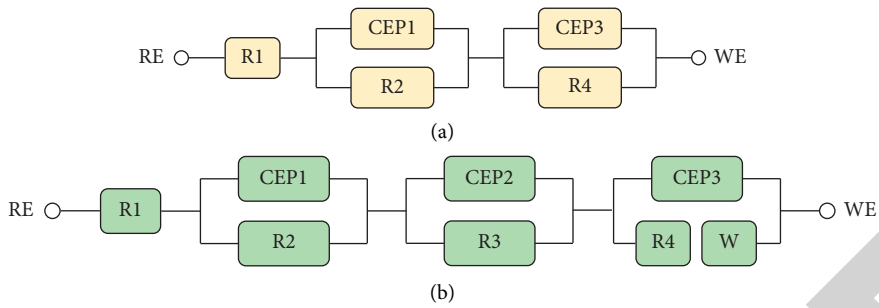

Figure 6: Equivalent circuit model under passivation and corrosion.

polyphase structure differences of the rock itself. Therefore, we use the angle-to-angle ratio (CPE) to simulate the rate and output behavior of two-layer electrodes to change the equilibrium of the electronic devices [25–30].

5. Conclusion

To investigate the special electrochemical process of corrosion improvement in seawater sand concrete in marine environment, this study used linear voltammetry (LSV) and electrochemical impedance spectroscopy (EIS) to elucidate the electrochemical mechanism and the rate of corrosion improvement in seawater sandstone by two yam, compared with ordinary stones, the following points can be drawn.

(1) The self-corrosion potential of seawater and sea sand concrete specimens increases gradually under two chloride ion corrosion modes, indicating that the subsequent corrosion reaction is more difficult with the aggravation of reinforcement corrosion degree. At the same time, the self-corrosion potential of steel bars in ordinary reinforced concrete in the soaking state gradually tends to be flat, indicating that it is always in a state of easy corrosion.

(2) When the steel bar in the rock is in a passive state, there are two capacitive reaction arcs, the capacitive reaction arc in the high-frequency region is the protective layer of rocks and the capacitive reaction arc in the low-frequency region is determined. Charge and release characteristics of two-layer electrodes on the surface of electrochemical steel bar. There are three capacitive reactance arcs in the Nyquist diagram, where the reinforcement in the sea rock and sea sand first corrodes, and the significance of the capacitive reactance arc in the high-frequency region, and in rare cases, it is the same, and the second new capacitive reactance arc in the medium-frequency region is an electrochemical characteristic of pitting corrosion.

(3) The arc radius of the reaction capacity in seawater and sand is always lower than that of normal rock, indicating that the chloride ions carried by its aggregates and water interactions mixed have a significant impact on the formation of weak rocks. The film on the surface of the armature is reflected in the parallel circuit, that is, the conduction also on the surface of the armature is reduced, and the anodic oxidation reaction is easier.

Data Availability

The data used to support the findings of this study are available from the corresponding author upon request.

Conflicts of Interest

The author declares that there are no conflicts of interest.

References

[1] T. Yu, J. F. Chen, J. Xiao, K. Zhang, J. Xiao, and Q. Zhang, "Experimental study on stress-strain curves of seawater sea-sand concrete under uniaxial compression with different strain rates," *Advances in Structural Engineering*, vol. 24, no. 6, pp. 1124–1137, 2021.

[2] V. Bhashya, G. Ramesh, S. S. Kumar, and B. Sangoju, "Performance evaluation of concretes by using recycled aggregate," *Indian Concrete Journal*, vol. 94, no. 1, pp. 51–57, 2020.

[3] G. Liu, B. Shan, D. Lai et al., "Seismic performance of seawater and sea sand concrete-filled ultra-high performance concrete tubes under low-cycle reversed lateral loading," *Advances in Structural Engineering*, vol. 24, no. 6, pp. 1221–1234, 2021.

[4] Y. L. Li, X. L. Zhao, R. S. Raman, Y. L. Li, X. L. Zhao, and R. S. Raman, "Durability of seawater and sea sand concrete and seawater and sea sand concrete–filled fibre-reinforced polymer/stainless steel tubular stub columns," *Advances in Structural Engineering*, vol. 24, no. 6, pp. 1074–1089, 2021.

[5] Z. Dong, G. Wu, X. L. Zhao, H. Zhu, and J. L. Lian, "The durability of seawater sea-sand concrete beams reinforced with metal bars or non-metal bars in the ocean environment," *Advances in Structural Engineering*, vol. 23, no. 2, pp. 334–347, 2020.

[6] Y. Huang, J. Xiao, L. Qin et al., "Mechanical behaviors of gfrp tube confined recycled aggregate concrete with sea sand," *Advances in Structural Engineering*, vol. 24, no. 6, pp. 1196–1207, 2021.

[7] Z. Dong, G. Wu, H. Zhu, Y. Wei, X. L. Zhao, and X. Shao, "Bond and flexural performance of basalt fiber–reinforced polymer bar–reinforced seawater sea sand glass aggregate concrete beams," *Advances in Structural Engineering*, vol. 24, no. 15, pp. 3359–3374, 2021.

[8] X. l. Fan, S. j. Gu, X. Wu et al., "Critical shear crack theory-based punching shear model for frp-reinforced concrete slabs," *Advances in Structural Engineering*, vol. 24, no. 6, pp. 1208–1220, 2021.

[9] W. Xin, S. Jianzhe, D. Lining et al., "Durability of coral-reef-sand concrete beams reinforced with basalt fibre-reinforced polymer bars in seawater," *Advances in Structural Engineering*, vol. 24, no. 6, pp. 1235–1247, 2021.

[10] G. Turuallo, H. Mallisa, and N. Rupang, "Sustainable development: using stone dust to replace a part of sand in concrete mixture," *MATEC Web of Conferences*, vol. 331, no. 1, pp. 05001–05007, 2020.

[11] Z. Kerrida, H. Berkak, Z. Makhloufi, M. Bederina, and A. Ferhat, "Effect of gravel-sand ratio on physico-mechanical, thermal and macro- structural properties of micro epoxy polymer concrete based on a mixture of alluvial-dune sand," *The Open Civil Engineering Journal*, vol. 14, no. 1, pp. 247–261, 2020.

[12] C. Sim, M. Tadros, D. Gee, and M. Asaad, "Flexural design of precast, prestressed ultra-high-performance concrete members," *PCI Journal*, vol. 65, no. 6, pp. 35–61, 2020.

[13] S. Takaya, R. Saito, S. Satoh, and T. Yamamoto, "Maintenance scenario of concrete structures damaged by reinforcement corrosion based on corrosion propagation mechanism of steel and moisture behavior in concrete," *Journal of Advanced Concrete Technology*, vol. 19, no. 6, pp. 614–629, 2021.

[14] H. Ueda, Y. Sakai, K. Kinomura, K. Watanabe, T. Ishida, and T. Kishi, "Durability design method considering reinforcement corrosion due to water penetration," *Journal of Advanced Concrete Technology*, vol. 18, no. 1, pp. 27–38, 2020.

[15] R. E. Melchers and I. A. Chaves, "Reinforcement corrosion in marine concretes—2 long-term effects," *ACI Materials Journal*, vol. 117, no. 2, pp. 217–228, 2020.

[16] P. Kuan, Q. Hongxia, and C. Kefan, "Study on corrosion of reinforcement bars in ceramic recycled gradient concrete," *Emerging Materials Research*, vol. 9, no. 1, pp. 1–7, 2020.

[17] S. S. D. Raavi and D. D. Tripura, "Predicting the effect of weathering and corrosion on the bond properties of bamboo- and steel-reinforced cement-stabilized rammed earth blocks," *Advances in Structural Engineering*, vol. 24, no. 14, pp. 3267–3280, 2021.

[18] C. N. Dacuan, V. Y. Abellana, and H. A. R. Canseco, "Assessment and evaluation of blended cement using bamboo leaf ash blash against corrosion," *Civil Engineering Journal*, vol. 7, no. 6, pp. 1015–1035, 2021.

[19] L. Liu, K. Pan, K. Xu, X. Peng, and J. Z. Zhang, "Synthesis and optical properties of mn 2+ -doped amino lead halide molecular clusters assisted by chloride ion," *Journal of Physical Chemistry Letters*, vol. 12, no. 31, pp. 7497–7503, 2021.

[20] T. Wang, J. Liu, and X. Cao, "Revealing the dynamic process of ion pair recognition by calix[4]pyrrole: a case study of cesium chloride," *Journal of Physical Chemistry Letters*, vol. 12, no. 13, pp. 3253–3259, 2021.

[21] Y. Nie, M. Xu, X. Zhang, M. Li, and Y. Song, "Polarization coupling based on faraday effect in whispering-gallery-mode resonator," *IEEE Photonics Journal*, vol. 12, no. 2, pp. 1–7, 2020.

[22] T. Irie, D. Morihashi, Y. Hirohata, and T. Haruna, "Polarization curves of carbon steel in concentrated libr solutions containing lioh and li2moo4 at different temperatures after short immersion," *Materials Transactions*, vol. 62, no. 3, pp. 420–426, 2021.

[23] C. Deng, H. Wang, and S. Wang, "Clarifying the lithium storage behavior of mos2 with in situ electrochemical impedance spectroscopy," *Journal of Materials Chemistry*, vol. 9, no. 28, pp. 15734–15743, 2021.

[24] R. Huang and X. Yang, "Analysis and research hotspots of ceramic materials in textile application," *Journal of Ceramic Processing Research*, vol. 23, no. 3, pp. 312–319, 2022.

[25] L. Kavan, M. Vinarcikova, M. Zlámalová, and M. Zukalova, "Titania containing cathodes for lithium-sulfur batteries: case studies by electrochemical impedance spectroscopy," *ECS Transactions*, vol. 105, no. 1, pp. 169–176, 2021.

[26] X. Zhang, K. P. Rane, I. Kakaravada, and M. Shabaz, "Research on vibration monitoring and fault diagnosis of rotating machinery based on internet of things technology," *Nonlinear Engineering*, vol. 10, no. 1, pp. 245–254, 2021.

[27] Z. Huang and S. Li, "Reactivation of learned reward association reduces retroactive interference from new reward learning," *Journal of Experimental Psychology: Learning, Memory, and Cognition*, vol. 48, no. 2, pp. 213–225, 2022.

[28] J. Chen, J. Liu, X. Liu, X. Xu, and F. Zhong, "Decomposition of toluene with a combined plasma photolysis (CPP) reactor: influence of UV irradiation and byproduct analysis," *Plasma Chemistry and Plasma Processing*, vol. 41, no. 1, pp. 409–420, 2021.

[29] P. Ajay and J. Jaya, "Bi-level energy optimization model in smart integrated engineering systems using WSN," *Energy Reports*, vol. 8, pp. 2490–2495, 2022.

[30] K. Sharma and B. K. Chaurasia, "Trust based location finding mechanism in VANET using DST," in *Proceedings of the Fifth International Conference on Communication Systems & Network Technologies*, pp. 763–766, Paris, France, 2015.